Femtosecond study of $Cu(H_2O)$ dynamics

Felician Muntean,[a] Mark S. Taylor, Anne B. McCoy,[b] and W. Carl Lineberger
JILA and Department of Chemistry and Biochemistry, University of Colorado, Boulder, Colorado 80309

(Received 3 May 2004; accepted 21 June 2004)

The short-time nuclear dynamics of $Cu(H_2O)$ is investigated using femtosecond photodetachment-photoionization spectroscopy and time-dependent quantum wave packet calculations. The $Cu(H_2O)$ dynamics is initiated in the electronic ground state of the complex by electron photodetachment from the $Cu^-(H_2O)$ complex, where hydrogen atoms are oriented toward Cu. Several time-resolved resonant multiphoton ionization schemes are used to probe the ensuing reorientation and dissociation. Immediately following photodetachment, the neutral complex is far from its minimum energy geometry and possesses an internal energy comparable to the Cu-H_2O dissociation energy and undergoes both large-amplitude H_2O motion and dissociation. Dissociation is observed to occur on three distinct time scales: 0.6, 8, and 100 ps. These results are compared to the results of time-dependent $J=0$ wave packet calculations, propagating the initial anion vibrational wave functions on the ground-state potential of the neutral complex. An excellent agreement is obtained between the experimental results and the ionization signals derived from the calculated probability amplitudes. Related experiments and calculations are carried out on the $Cu(D_2O)$ complex, with results very similar to those of $Cu(H_2O)$. © *2004 American Institute of Physics.* [DOI: 10.1063/1.1782176]

I. INTRODUCTION

Both intermolecular energy transfer and solvation dynamics play pivotal roles in chemical reactions in the condensed phase.[1,2] Dynamic solvent-solute interactions have been shown to be important in governing the rates of both electron transfer reactions[3] and reactions involving bond making and breaking.[4] Femtosecond pump-probe laser spectroscopy is a powerful technique for examining intermolecular energy transfer and solvation dynamics in both the condensed phase[5–7] and within neutral or ionic clusters.[8–12] In this study, we employ femtosecond pump-probe laser spectroscopy and quantum dynamical calculations to examine the H_2O reorientation and dissociation dynamics within a $Cu(H_2O)$ complex that is produced by photodetachment of $Cu^-(H_2O)$.

In related studies, femtosecond pump-probe spectroscopy has been used to investigate solvation dynamics in both neutral[8,9] and anionic[10–15] gas-phase complexes. The femtosecond photodetachment-photoionization experiments reported here exploit the fact that a polar molecule in a binary complex with an atomic metal anion will undergo large-amplitude reorientation and dissociation following electron photodetachment. Elementary chemical principles and high-level *ab initio* calculations concur that $Cu^-(H_2O)$ is planar with the hydrogen atoms oriented toward the copper anion, while neutral $Cu(H_2O)$ has the oxygen oriented toward copper and a diminished Cu-OH_2 separation (Fig. 1) compared to the anion. Electron photodetachment of $Cu^-(H_2O)$ produces neutral $Cu(H_2O)$ initially at the anion geometry with an internal energy that is near the Cu-H_2O dissociation energy. Immediately after the birth of neutral $Cu(H_2O)$, the water molecule will begin to rotate and vibrate with respect to Cu, and a fraction of the complexes will dissociate. We expect the dissociation to have both direct and delayed components, the latter arising from coupling between the internal rotation of H_2O and the Cu-H_2O stretching vibration. Classical[16] and quantum[17] dynamics calculations have predicted that similar behavior will be exhibited by the complexes $Cl(H_2O)$ and $Br(H_2O)$ prepared by electron photodetachment of their anionic precursors. Analogous energy transfer dynamics resulting in direct and delayed dissociation has been observed within the Hg-N_2 complex.[18] Using picosecond laser pump-probe spectroscopy, Soep and co-workers observed[18] both direct and delayed dissociation following electronic excitation of Hg-N_2. They concluded that energy flow from internal rotation of N_2 into the Hg-N_2 stretching vibration was responsible for the delayed dissociation. The present joint time-resolved experimental and theoretical study extends such investigations to solvation dynamics occurring on the electronic ground state of a van der Waals complex. The work described here is also closely related to the elegant dissociative photodetachment experiments carried out by Continetti.[19,20] These experiments obtain a complementary view of dissociation dynamics by employing photoelectron-photofragment coincidence spectroscopy to obtain detailed information concerning the dissociation dynamics. Several comprehensive reviews of this approach have recently appeared.[21,22] Of particular relevance to the experiments reported here are studies of solvated O^-, OH^-, and O_2^- anions.[23–27]

In this work, electrons are photodetached from a mass-selected beam of $Cu^-(H_2O)$ by a 400 nm, 120 fs laser pulse,

[a]Permanent address: Varian Corporation, Walnut Creek, CA.
[b]Permanent address: Department of Chemistry, The Ohio State University, Columbus, OH.

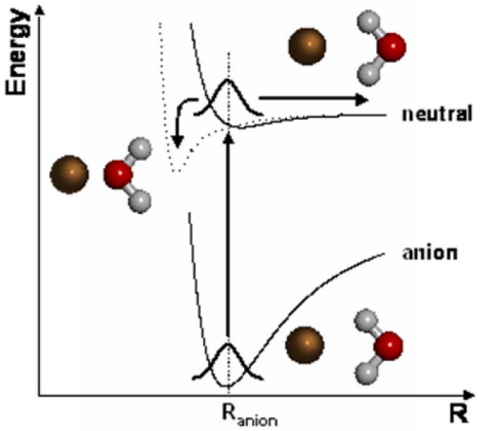

FIG. 1. Schematic illustration of the $Cu(H_2O)$ dynamics upon electron photodetachment of the negative ion.

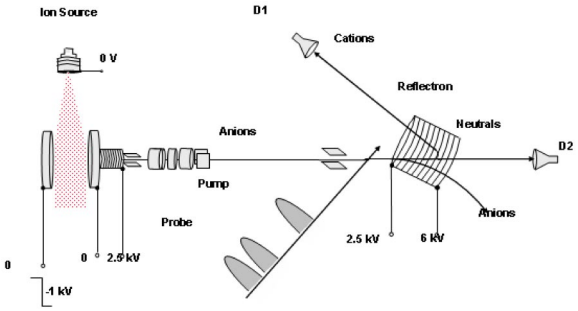

FIG. 2. Schematic diagram of the ion beam portion of the photodetachment-photoionization apparatus.

preparing an ensemble of time-evolving $Cu(H_2O)$ complexes. Delayed resonance enhanced multiphoton ionization (REMPI) is used to follow the time evolution of the neutral complexes and their dissociated fragments. This experimental approach offers advantages over other femtosecond pump-probe techniques used for studying the dynamics of gas-phase neutral molecules. Starting with a negative ion allows mass selection and enables the formation of a neutral complex with a well-defined initial nuclear configuration. Photodetachment of negative ions initiates the dynamics on the electronic ground state of the neutrals, while avoiding the complexity inherent in coherent nonlinear techniques used to initiate ground state dynamics.[28,29] Probing by time-delayed REMPI allows for simultaneous detection of the parent complex and dissociated products by secondary mass analysis. Wöste and co-workers developed time-resolved photodetachment-photoionization spectroscopy[30] and used it to study the rearrangement dynamics of neutral Ag_3. Their approach was modified in our laboratory by replacing the slow ion beam and quadrupole ion trap with a pulsed supersonic expansion ion source and fast ion beam, and it was also used to investigate the rearrangement dynamics of Ag_3.[31] These developments allowed production of colder negative ions and simultaneous detection of both neutral and positive ion photoproducts. The work from our laboratory[31] and subsequent theoretical studies[32–34] emphasized that the time evolution of the photodetachment-photoionization signals is caused not only by nuclear dynamics on the ground-state potential energy surface but also by the involvement of intermediate electronically excited states in the REMPI process.

We choose to study the H_2O reorientation dynamics and energy redistribution in the $Cu(H_2O)$ complex for several reasons. First, both simple chemical principles and *ab initio* calculations[35,36] predict the equilibrium geometries of the anion and neutral complexes to differ significantly (Fig. 1). Negative ion photoelectron spectroscopy[37,38] and calculations[35,36] agree that $Cu^-(H_2O)$ is well described as a hydrated copper atomic anion and that it has a vertical detachment energy of about 1.6 eV. Electron photodetachment using the second harmonic of the Ti:sapphire laser (398 nm, 3.12 eV) will produce neutral $Cu(H_2O)$ primarily in its ground electronic state. The ground state of copper has an alkali-like electronic structure, $^2S_{1/2}$ $(3d^{10}4s^1)$, which gives rise to two strong $^2P_{1/2,3/2}\leftarrow{}^2S_{1/2}$ transitions at 327 and 325 nm, respectively. Both calculations[35] and related spectroscopic studies[39–42] suggest that these transition energies will shift markedly with the H_2O orientation and Cu-H_2O separation. Ionizing the complex using varying excitation energies will thus probe the cluster in different transient nuclear configurations.[35] The approach we take has two components. First, femtosecond photodetachment-photoionization experiments are used to investigate the evolution of $Cu(H_2O)$ for the first 100 ps following photodetachment of $Cu^-(H_2O)$. Second, the dynamics of $Cu(H_2O)$ are simulated by quantum wave packet calculations: the $Cu^-(H_2O)$ vibrational wave functions populated under the experimental conditions are propagated quantum mechanically on the neutral $Cu(H_2O)$ surface. Details of the $Cu^-(H_2O)$ and $Cu(H_2O)$ potential energy surfaces and vibrational wave functions evaluated from these surfaces are presented in the following paper.[35] The remainder of this paper is structured as follows. We present our experimental methods and apparatus in Sec. II. In Sec. III, we describe the theoretical and computational methodology used to calculate the time-dependent dynamics of $Cu(H_2O)$. We present the results of our femtosecond photodetachment-photoionization experiments on $Cu(H_2O)$ in Sec. IV. In Sec. V, the dynamics of $Cu(H_2O)$ are discussed and interpreted in light of the experimental observations and the time-dependent wave packet calculations.

II. EXPERIMENT

The time-resolved photodetachment-photoionization of $Cu^-(H_2O)$ is performed using the charge-reversal instrument described previously,[31] so only relevant details will be given here.

A. Ion production, transport, and product analysis

A schematic of the ion-beam part of the apparatus is presented in Fig. 2. A high-pressure pulsed sputtering discharge ion source[31] is used to make $Cu^-(H_2O)_n$ cluster ions. A mixture of 80% Ne and 20% Ar at stagnation pressures between 6 and 8 atm flows through a small water container at room temperature and expands into vacuum through a pulsed (200 Hz) General Valve (0.8 mm orifice, Parker Hannifin). A sputtering discharge is initiated when the gas pulse flows

past a negative 2–3 kV potential between a copper rod cathode and a stainless steel rod at ground potential. The $Cu^-(H_2O)$ complexes are produced in the high-pressure region immediately following the discharge, inside a 3 mm diameter source channel. They are further cooled and stabilized downstream, inside the cone-shaped expansion channel, and then allowed to expand into the $(0.5–1.0)\times10^{-4}$ Torr pressure of the source chamber. Along with $Cu^-(H_2O)_n$ ions, the source generates Cu_n^-, $CuO^-(H_2O)_n$, $CuOH^-(H_2O)_n$, $O^-(H_2O)_n$, and $OH^-(H_2O)_n$. In order to avoid mass contamination of $^{63}Cu^-(H_2O)$ with $^{65}CuO^-$, we study the less abundant, but isotopically pure, m/z 83 ion packet [$^{65}Cu^-(H_2O)$], and for the deuteration experiments we employ m/z 85 [$^{65}Cu^-(D_2O)$]. The rotational and vibrational temperatures of the anions made in this source are not well characterized. Previous studies of large cluster ions[43,44] indicated that they both range between 40 and 60 K. For these smaller clusters, we expect both to be higher, possibly 100–200 K.

At 10 cm below the nozzle, a pulsed transverse electric field extracts the negative ions into a differentially pumped Wiley-McLaren[45] time-of-flight mass spectrometer (Fig. 2). They are further accelerated to ~3 keV energy, and brought to a spatial and temporal focus at the photodetachment region 1.8 m downstream. The fast neutrals produced by the photodetachment pulse are detected by an in-line channeltron detector. The cation products enter a reflectron mass spectrometer and are subsequently counted with an off-axis microchannel-plate detector. This dual collector arrangement enables the normalization of the cation signal to the neutral signal, which is found to be very helpful for reducing the effects of fluctuations in the negative ion intensity and flight time.

B. Laser system

Most of the femtosecond laser system has been extensively described.[31,44] A Ti:sapphire oscillator (Coherent Mira Basic) pumped by a Nd:VO_4 laser (Coherent Verdi V5) produces ~85 fs pulses at 750–850 nm. The pulses are amplified by a regenerative, multipass Ti:sapphire amplifier (Quantronix Titan), pumped by a Nd:YLF laser (Quantronix, model 527 DQ), to 3 mJ/pulse and 120 fs, at a repetition rate of 400 Hz. Two-thirds of this infrared light is used to generate second harmonic (398 nm) and third harmonic (265 nm) (CSK Optronics Supertripler, model 8315A) radiation, while the remainder pumps an optical parametric amplifier (OPA, Light Conversion TOPAS), whose fourth harmonic output provides tunable radiation between 300 and 400 nm. Finally, the OPA and the 398 nm pulses pass through delay stages and are further combined with the 265 nm pulse in a collinear configuration. All three pulses are focused to a spot of ~1 mm diameter at the point of interaction with the ion packet, where their typical energies are 100 μJ for 398 nm, 60 μJ for 265 nm, and 10–12 μJ for the OPA.

C. Measurements performed

We investigate the dynamics of the $Cu(H_2O)$ complex through four time-resolved photodetachment-photoionization measurements. For all measurements reported here, the neutral $Cu(H_2O)$ complex is formed by electron photodetachment from $Cu^-(H_2O)$ using a 398 nm pulse and the cation signal is recorded as a function of the delay between the photodetachment and the excitation/ionization pulses (OPA/265 nm). The four ionization schemes are described below and three are shown schematically in Fig. 3. In this figure, the various laser pulse sequences are superimposed upon a schematic, partial potential energy diagram[46] displaying the electronic states involved in the experiments.

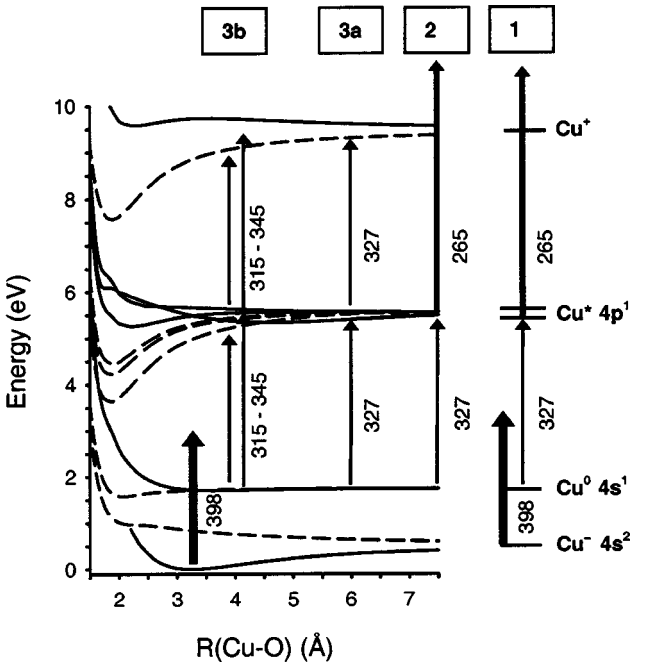

FIG. 3. Schematic representation of the measurements performed, as described in the text. Dotted lines represent cuts in the Cu-OH_2 C_{2v} configurations, while solid lines show cuts in the Cu-H_2O C_{2v} geometry.

1. Three-color photodetachment photoionization of Cu^-

The time resolution of the experimental apparatus is determined *in situ*, using three-color, three-photon photodetachment photoionization of Cu^- (Fig. 3, scheme 1),

$$Cu^- \xrightarrow{398\ \text{nm}\ (t=0)} Cu \xrightarrow{327+265\ \text{nm}\ (t=\Delta t)} \text{detect}\ Cu^+. \qquad (1)$$

The 398 nm pulse photodetaches an electron from Cu^- and a sequence of 327 and 265 nm photons resonantly ionize the $^2S_{1/2}$ Cu atom through the $^2P_{1/2}$ intermediate state. The delay between the excitation and the ionization (265 nm) pulses is fixed at 0.3 ps. As the photodetachment–resonant photoionization delay time (Δt) is varied, the Cu^+ signal exhibits a step function increase at $\Delta t=0$ (Fig. 4) and the rise time of this step gives a direct measurement of the time resolution of the apparatus. The solid line in Fig. 4 is a fit of the data to the form $A[1+\tanh(t/\tau)]$ and the derivative of this fit (dashed line) has a sech^2 form. The width [full width at half maximum (FWHM)] of this sech^2 function provides the effective time resolution of the experimental apparatus, 260 fs.

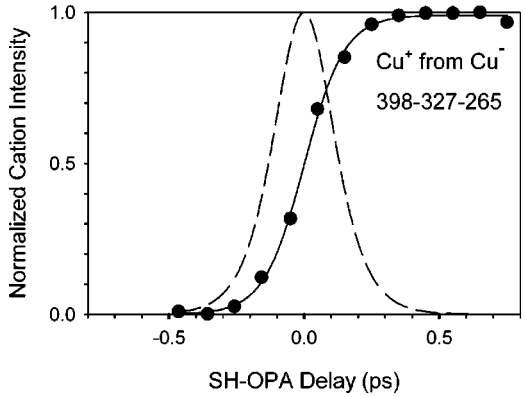

FIG. 4. The three-color photodetachment photoionization of Cu^- with 398, 327, and 265 nm laser pulses as a function of the time delay between the photodetachment (398 nm) and the resonant excitation (327 nm) pulses. The solid line represents a tanh fit to the data and the dashed line is the derivative ($sech^2$) of the fit, an *in situ* measurement of the effective time resolution of the experiment.

2. Two-color resonant ionization of Cu arising from dissociative photodetachment of $Cu^-(H_2O)$

The Cu atom fragment resulting from dissociative photodetachment is monitored as a function of the delay time between the photodetachment photon (398 nm) and the $^2P_{1/2} \leftarrow {}^2S_{1/2}$ excitation of the copper atom by a 327 nm photon (Fig. 3, scheme 2),

$$\mathrm{Cu^-(H_2O)} \xrightarrow{398\ \mathrm{nm}\ (t=0)} \mathrm{Cu(H_2O)} \xrightarrow{t=\Delta t} \mathrm{Cu+H_2O} \xrightarrow{327+265\ \mathrm{nm}} \mathrm{detect\ Cu^+ + H_2O}. \quad (2)$$

The delay between the resonant excitation (327 nm) pulse and the ionization (265 nm) pulse is fixed at 0.3 ps. This is exactly the same measurement process described above, except that the laser pulses intersect $Cu^-(H_2O)$, rather than Cu^-. The major background contribution is from two-color (327 and 265 nm) photodetachment photoionization of $Cu^-(H_2O)$ and is typically 10% of the maximum of the three-color signal.

3. One-color, resonant multiphoton ionization of initially bound $Cu(H_2O)$

The bound $Cu(H_2O)$ complex is probed, as a function of time after photodetachment, by one-color multiphoton ionization using a tunable (OPA) pulse (Fig. 3, scheme 3),

$$\mathrm{Cu^-(H_2O)} \xrightarrow{398\ \mathrm{nm}\ (t=0)} \mathrm{Cu(H_2O)} \xrightarrow{t=\Delta t} \mathrm{Cu(H_2O)} \xrightarrow{2\times(315-345)\ \mathrm{nm}} \mathrm{detect\ Cu^+(H_2O)}. \quad (3)$$

The excitation wavelength is tuned over the range 315–345 nm. The major background contribution is from one-color (OPA) photodetachment-photoionization of Cu^-, and is typically 20% of the maximum of the two-color (398 OPA) signal.

4. One-color dissociative multiphoton ionization of initially bound $Cu(H_2O)$

This measurement is the same as the one above, except that it is a higher order multiphoton process, and the ion detected is Cu^+

$$\mathrm{Cu^-(H_2O)} \xrightarrow{398\ \mathrm{nm}\ (t=0)} \mathrm{Cu(H_2O)} \xrightarrow{t=\Delta t} \mathrm{Cu(H_2O)} \xrightarrow{3\times(315-345)\ \mathrm{nm}} \mathrm{detect\ Cu^+ + H_2O}. \quad (4)$$

The one-color ionization used here does not allow efficient multiphoton ionization of the isolated Cu atom, even when the OPA is tuned to the 327 nm Cu atom resonance transition. At that color, the energy of two 327 nm photons (7.58 eV) is insufficient to ionize the isolated Cu atom [ionization potential (IP) = 7.73 eV]. In contrast with the two-color resonant ionization of the neutral Cu fragment arising from dissociative photodetachment, the Cu^+ cation signal in this case comes from dissociative photoionization of the $Cu(H_2O)$ complex. The Cu^+ time dependence observed in this process is essentially the same as that observed for the $Cu^+(H_2O)$ produced by one-color multiphoton ionization of $Cu(H_2O)$.

D. Experimental details and data acquisition

Optimal laser-ion spatial overlap is of primary importance for our two- and three-color experiments. The optimal overlap is best achieved through the optimization of the photodetachment photoionization of Cu^- in a two-step procedure. First, the photodetachment (398 nm) pulse is positioned in time and space to maximize the Cu neutral signal. The resonant excitation (327 nm) OPA and the ionization 265 nm pulses are introduced and adjusted spatially to maximize the Cu^+ cation signal. Special care is also taken to ensure that the laser modes are as uniform as possible in the far field, in the region of interaction with the ions. Typically, 5%–10% of the parent negative ion beam is photodetached by the 398 nm radiation, but a significantly smaller proportion of the photodetached neutrals are themselves ionized by the subsequent pulses.

The data acquisition procedure consists of scanning a range of time delays between the 398 nm pulse and the fixed OPA and 265 nm pulses, while simultaneously measuring the total [both intact $Cu(H_2O)$ and dissociated neutral products] neutral signal and the individual Cu^+ and $Cu^+(H_2O)$ product cation signals. One single scan consists of sweeping the entire range of time delays while data are accumulated during 800 laser shots per time delay. Many back and forth scans are performed for a total of 20 000–40 000 laser shots per time delay. This procedure allows continuous monitoring of the measured signals at all time delays to check for any major drift. The final signal (after appropriate background corrections) is given by the cation signal divided by the neutral signal. Although we do not continuously monitor the intensities of the ionizing laser pulses during data acquisition, we periodically check their intensities and spatial positions.

The maximum $Cu^+(H_2O)$ and Cu^+ count rates are about 0.2 and 0.5 counts/laser shot, respectively. The principal challenge of the experiment arises from maintaining stability during the several hours of signal optimization and data acquisition. It is especially challenging to maintain a stable spatial overlap of the three laser beams and the ion packet, due to the variations of the pulsed valve operation and to the slight pointing drift of the three laser beams as the room temperature changes. Background signals due to the individual photodetachment or photoionization pulses are typically recorded at the beginning and end of data acquisition and are subtracted from the time-dependent signals.

III. THEORY

From a theoretical standpoint, the photodetachment-photoionization dynamics of the $Cu(H_2O)$ complex can be considered in three parts. The first part involves the characterization of $Cu^-(H_2O)$ and is described in the following paper.[35] In the second part, the photodetachment process will be modeled assuming a constant transition moment and an infinitely sharp laser pulse. As such, in this step of the calculations, we take a set of vibrational wave functions for the anion and propagate each of them on the neutral surface, using standard time-dependent approaches.[47–49] Finally, the ionization process needs to be considered. We use *ab initio* calculations of the electronic excitation and ionization energies of $Cu(H_2O)$, as described in the following paper,[35] to determine the configurations for which the system is most likely to be ionized and analyze the results of the simulations according to this model. Excitation energies are determined for transitions between the ground electronic state and those excited electronic states that correlate the $^2P_{1/2,3/2}$ states of Cu and ground-state H_2O.

A. Coordinates and Hamiltonian

As the intramolecular vibrations of water are fast compared to the intermolecular vibrational motions of $Cu(H_2O)$ in all of the states that are probed by the experiment, we will consider the potential and the dynamics in terms of the three intermolecular coordinates only. These three coordinates are the distance between the copper atom and the center of mass of the water, R, and the two orientation angles of the water molecule relative to the vector along R, θ, and ϕ (see following paper for details). We take as our reference geometry the configuration in which all four atoms lie in a plane and R lies along the C_2 axis of the water molecule, i.e., $\phi=0°$ and $\theta=90°$. Motion along θ corresponds to rotation of the water molecule out of the plane of the complex, while motion along ϕ corresponds to rotation in the plane of the complex.

In this representation of the copper-water complex, the Hamiltonian is given by

$$\begin{aligned}\hat{H} &= -\frac{\hbar^2}{2\mu_R}\frac{\partial^2}{\partial R^2} + \frac{2\pi c}{\hbar}[b_x\hat{j}_x^2 + b_y\hat{j}_y^2 + b_z\hat{j}_z^2] \\ &\quad + \frac{|\hat{J}-\hat{j}|^2}{2\mu_R R^2} + V(R,\theta,\phi) \\ &= -\frac{\hbar^2}{2\mu_R}\frac{\partial^2}{\partial R^2} + \frac{2\pi c}{\hbar}\left[\frac{b_x+b_y}{2}(\hat{j}^2-\hat{j}_z^2)\right. \\ &\quad \left. + \frac{b_x-b_y}{4}(\hat{j}_+^2+\hat{j}_-^2) + b_z\hat{j}_z^2\right] + \frac{|\hat{J}-\hat{j}|^2}{2\mu_R R^2} + V(R,\theta,\phi).\end{aligned} \tag{5}$$

Here, μ_R represents the reduced mass of the copper-water complex, while the b_α give the vibrationally averaged rotational constants of water. A mass of 62.929 599 amu was used for Cu, 15.994 915 amu for O, and 1.007 825 amu for H (2.014 102 amu for D). In the present coordinate system, $b_x=27.88$, $b_y=14.51$, and $b_z=9.28\ cm^{-1}$ for H_2O and $b_x=15.25$, $b_y=7.30$, and $b_z=4.94\ cm^{-1}$ for D_2O.[35] Finally, V represents the intermolecular potential for this system, described in detail in the following paper.[35]

B. Dynamics

In order to investigate the dynamics of the copper-water complex, we start the system in one of the vibrational eigenstates of the anion. We assume a constant electron photodetachment transition moment, and solve the time-dependent Schrödinger equation for each of the ten lowest energy vibrational states of $Cu^-(H_2O)$ and $Cu^-(D_2O)$. In all cases, the system is propagated to 9.6 ps, through a series of 8000, 50 a.u. (1.2 fs) time steps. In order to evaluate

$$\Psi(R,\theta,\phi,t+\Delta t) = e^{-i\hat{H}\Delta t/\hbar}\Psi(R,\theta,\phi,t), \tag{6}$$

we express the Hamiltonian matrix in terms of a low-order Lanczos recursion, consisting of 50 vectors that are initiated using $\Psi(R,\theta,\phi,t)$. We solve for the eigenvalues and eigenvectors of this system and use them to evaluate Eq. (6).[50,51] For these calculations, the wave functions are expressed in an evenly spaced grid of 500 points in R, ranging from 1.03 to 12.99 Å, while the angular dependence is expanded in spherical harmonics with $j\leqslant 10$ for $Cu(H_2O)$ and $j\leqslant 15$ for $Cu(D_2O)$.

Since as much as 65% of the wave packet will reach the asymptotic region of the potential in 10 ps, we multiply the part of the wave function for which $R>R_{abs}=10.34$ Å by a damping factor:[52]

$$a(R) = \exp[-2e^{-2(R_{\max}-R_{abs})/(R-R_{abs})}] \tag{7}$$

at each time step, where $R_{\max}=12$ Å. This choice ensures that there will not be any reflection of the wave packet off of the edge of the grid. As our analysis does not involve the parts of the wave packets that have amplitude at $R>8$ Å, we do not require detailed information about this portion of the wave functions.

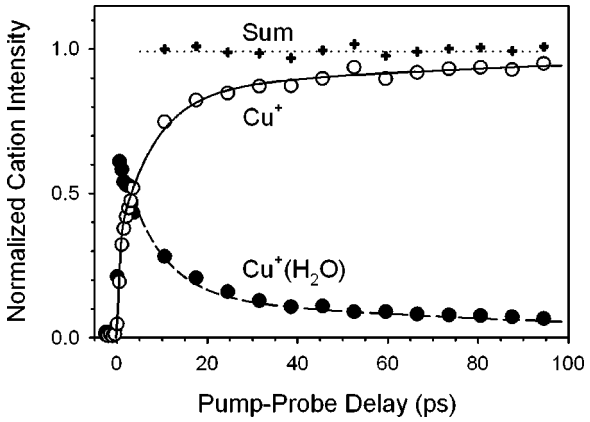

FIG. 5. Experimental time dependence of the photodetachment photoionization of $Cu^-(H_2O)$. The Cu^+ signal (hollow circles) is a result of 398 nm photodetachment followed by two-color (327+265 nm) resonant ionization (Fig. 3, scheme 2). The $Cu^+(H_2O)$ signal (black circles) is a result of 398 nm photodetachment followed by one-color (327 nm) resonant multiphoton ionization (Fig. 3, scheme 3).

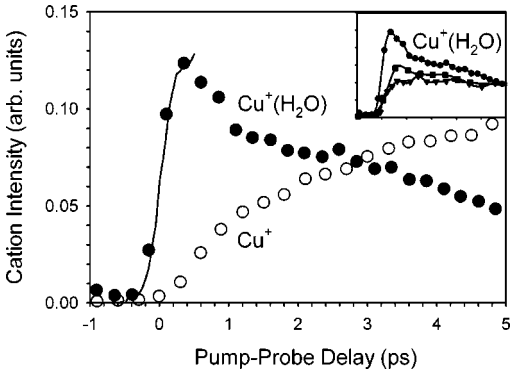

FIG. 6. Experimental time dependence of the photodetachment photoionization of $Cu^-(H_2O)$ in the first 5 ps after photodetachment. Measurement schemes are the same as those in Fig. 5. The inset shows several $Cu^+(H_2O)$ data sets that reflect the possible range of the early time signal variation observed under a range of source conditions.

IV. RESULTS

We divide our description of the results of Cu(H_2O) experiments into those in which the probe pulse is tuned to the Cu $^2P_{1/2}\leftarrow{}^2S_{1/2}$ transition (327 nm) and those in which it is tuned off this resonance (315–345 nm). The former experiments preferentially probe bound Cu(H_2O) at large copper-water separations [Fig. 3, scheme 3(a)] and dissociated Cu atoms (Fig. 3, scheme 2). The latter experiments probe bound Cu(H_2O) at smaller copper-water separations [Fig. 3, schemes 3(b)]. In addition, we present the results of analogous experiments on Cu(D_2O). Finally, we discuss the fitting procedures employed to extract characteristic times from the observed time dependences.

A. Dissociative photodetachment of $Cu^-(H_2O)$

1. Probing on the atomic Cu $^2P_{1/2}\leftarrow{}^2S_{1/2}$ resonance (327 nm)

These experiments probe the Cu atom photofragment as described in Sec. II C 2 and depicted by scheme 2 in Fig. 3. Analysis of the potential curves in Fig. 3 suggests that bound Cu(H_2O) will be resonantly ionized by multiple 327 nm photons when it samples Cu-H_2O separations in excess of $\sim$5.5 Å. This process is described in Sec. II C 3 and depicted as scheme 3(a) in Fig. 3. This ionization window spans a restricted range of radial separations, because two 327 nm photons (7.58 eV) can only ionize the bound Cu(H_2O) complex in certain water orientations and they have insufficient energy to ionize the isolated Cu atom (IP=7.73 eV).

The time dependence of the Cu^+ signal for 100 ps after electron photodetachment from $Cu^-(H_2O)$ is presented in Fig. 5. The Cu^+ signal exhibits at least three distinct dissociation time scales during the 100 ps observation period. It rises rapidly during the first picosecond, more slowly for the next several picoseconds, continues to rise at an even slower rate, and is still increasing slowly after 100 ps. The $Cu^+(H_2O)$ signal, also presented in Fig. 5, exhibits a complementary behavior. It rises rapidly and decays over $>$10 ps and a single exponential cannot be used to describe its decay. The sum of the two signals is a constant function of the photodetachment-photoionization delay time. This indicates that the two signals have similar characteristic time constants at times longer than 5 ps and suggests that the Cu^+ signal results from dissociation of neutral Cu(H_2O), followed by resonant ionization of the Cu atom.

Figure 6 displays the onsets of the two signals in the first 5 ps following electron photodetachment from $Cu^-(H_2O)$. The solid line represents the Cu^+ signal from the photodetachment-photoionization of Cu^- (Fig. 3, scheme 1) and indicates the time resolution of our experiment. The $Cu^+(H_2O)$ signal rises at the same rate, which indicates that neutral Cu(H_2O) is ionized at pump-probe delay times smaller than the 260 fs experimental resolution. In contrast, the Cu^+ onset is both resolvable and delayed with respect to the photodetachment event. Weak oscillatory features are observed in the $Cu^+(H_2O)$ signal after very long averaging times. We are currently studying these features and they will be discussed in a future publication.

The relative magnitude of the fast rise of the Cu^+ signal with respect to the maximum signal at long time exhibits modest variability ($\sim$10% of the signal's asymptotic value) between data sets taken on different days. The initial part of the $Cu^+(H_2O)$ signal, the first 5–6 ps, is observed to vary substantially between data sets from a pronounced decay with a faster component in the first 1–1.5 ps to a flat time dependence, as displayed in the inset in Fig. 6. This variation is partly attributed to changes in laser (OPA) focusing: stronger focusing is found to yield $Cu^+(H_2O)$ signals with more pronounced initial decays, and partly attributed to a day-to-day variation in anion temperatures with varying ion source conditions. At times longer than the first 5–6 ps, all $Cu^+(H_2O)$ data sets exhibit the same time dependence.

The overall magnitude of the $Cu^+(H_2O)$ signal compared to the Cu^+ signal can change substantially (up to a factor of 8) between data sets. This latter variation is consistent with a multiphoton OPA process producing the $Cu^+(H_2O)$ signal, in contrast with a one-photon OPA process producing the Cu^+ signal.

Finally, we note that the $Cu^+(H_2O)$ signal produced by absorption of one 327 nm photon and one 265 nm photon is

more than an order of magnitude smaller than the two-photon 327 nm signal described above. This result is obtained even though the 265 nm pulse typically has five times the number of photons as the 327 nm OPA pulse. This observation remains valid when the time delay between the excitation (327 nm) and the ionization (265 nm) pulses is varied over the range 0–3 ps. The weak $Cu^+(H_2O)$ signal obtained with the two-color (327–265 nm) ionization scheme precluded detailed analysis of its time dependence.

2. Probing off the atomic Cu $^2P_{1/2}\leftarrow{}^2S_{1/2}$ resonance (315–345 nm)

Inspection of the intermediate state(s) in Fig. 3 shows that tuning the OPA wavelength off the 327 nm Cu atom resonant transition moves the excitation window to smaller Cu-H_2O separations. When the second photon absorbed by the neutral complex is also an OPA photon, ionization is energetically possible only for restricted angular orientations of the water molecule. Thus $Cu^+(H_2O)$ formed by absorption of two OPA photons arises from absorption in a restricted angular and radial range [Fig. 3, scheme 3(b)]. The corresponding Cu^+ signals arise from dissociative multiphoton ionization of $Cu(H_2O)$. Such experiments were carried out detecting the ionic products following excitation at 315, 327, 330, 335, 340, and 345 nm. A similar measurement using the more intense, but nonresonant, 265 nm third harmonic radiation was also attempted, but no cation signals above background levels were detected.

Figure 7 shows the $Cu^+(H_2O)$ and Cu^+ transient signals obtained at excitation energies below (340 nm), on (327 nm), and above (315 nm) the Cu atom resonance transition. There are no significant differences (within our experimental scatter) between the time dependences of the $Cu^+(H_2O)$ signals at any of the wavelengths mentioned above (315–345 nm). The Cu^+ signals depicted in Fig. 7 have a completely different shape than seen in Figs. 5 and 6. The reason is that the latter arise from dissociative photodetachment of $Cu^-(H_2O)$, while the Cu^+ signals in Fig. 7 arise from dissociative multiphoton photoionization of $Cu(H_2O)$. Indeed, the observed Cu^+ signals are directly proportional to the corresponding $Cu^+(H_2O)$ signal. The $Cu^+/Cu^+(H_2O)$ ratio increases with increasing excitation energy, indicating that the $Cu^+(H_2O)$ dissociation fraction increases with increasing energy of the ionization photons.

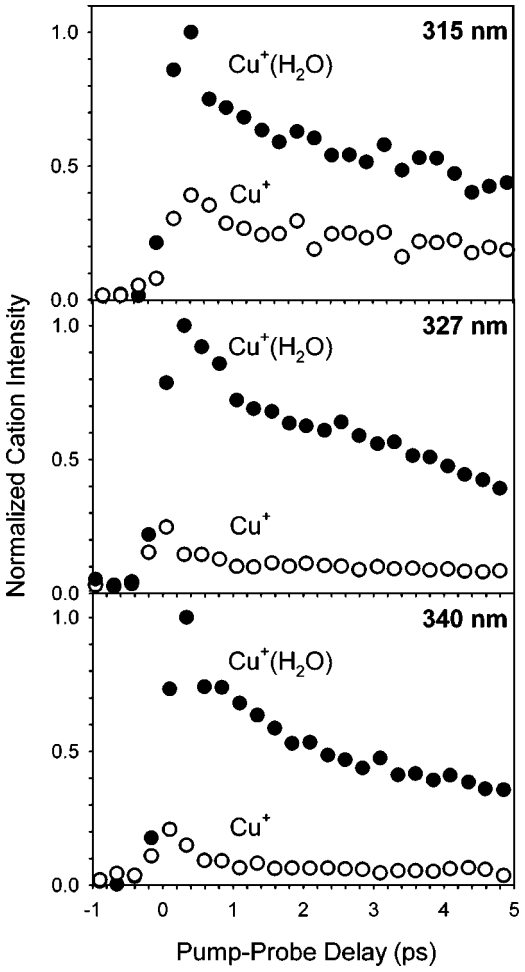

FIG. 7. Experimental time dependence of the photodetachment photoionization of $Cu^-(H_2O)$ at different resonant ionization wavelengths. The $Cu^+(H_2O)$ signal is a result of 398 nm photodetachment followed by one-color resonant multiphoton ionization with 315 nm (top), 327 nm (middle), and 340 nm (bottom). The Cu^+ cation signals detected at each wavelength are a result of dissociative ionization of $Cu(H_2O)$.

B. Effect of deuteration

Similar photodetachment-photoionization experiments are performed on $Cu^-(D_2O)$, using the same laser wavelengths and the same photodetachment-photoionization schemes as for the $Cu^-(H_2O)$ experiments. Data from the two isotopes are very similar, leading us to conclude that deuteration effects on the time dependences of the Cu^+ and $Cu^+(H_2O)$ cation channels are less than the current uncertainties of our measurements.

C. Fitting the time dependences

In order to extract characteristic time constants from the transients observed, we tested several fitting procedures. All of the fits are constrained to a model that assumes that the long-time dependences of the Cu^+ and the $Cu^+(H_2O)$ signals are complementary to one another, so that, as observed in Fig. 5, their sum is a constant. The simplest function employed, a single exponential [decay for the $Cu^+(H_2O)$ signal and rise to a maximum for the Cu^+ signal], does not fit satisfactorily the time evolution to 100 ps. This is not surprising, considering that our data clearly show more than one dissociation time scale (Figs. 5 and 6). Next, we try a sum of exponential functions, which would correspond to parallel dissociation processes. For the Cu^+ channel, a good fit is obtained with a sum of three increasing components,

$$I_{rise}=I_1\left[0.5+0.5\tanh\left(\frac{t-t_0}{\tau_1}\right)\right]+I_2[1-e^{-(t-t_0)H(t-t_0)/\tau_2}]+I_3[1-e^{-(t-t_0)H(t-t_0)/\tau_3}], \quad (8)$$

where $H(t-t_0)$ represents the Heaviside step function. The tanh function describing the most rapidly rising component τ_1 is chosen to have a form qualitatively related to the expected direct Cu–H_2O dissociation component. For the

TABLE I. The fit parameters used to model the time dependence of the cation signals.

	I_1[a]	I_2	I_3	τ_1 (ps)	τ_2 (ps)	τ_3 (ps)	t_0 (ps)
$Cu^-(H_2O)$/ $Cu^-(D_2O)$ Experiment[b]	0.35 (0.15)	0.5 (0.2)	0.15 (0.05)	0.6 (0.2)	8 (1)	100 (30)	0.4 (0.1)
$Cu^-(H_2O)$/ $Cu^-(D_2O)$ Calculation[c]	0.25	0.75	⋯	0.25	3.1	⋯	0.8

[a]The parameters are defined in Eqs. (8) and (9) and the values of I_1, I_2, and I_3 are constrained to sum to one.
[b]The H_2O and D_2O data were fit to the same set of constants. The number in parentheses represents the range of values obtained by fitting 11 different measured signals.
[c]Fit to the calculated signals calculated for a 200 K vibrational temperature of $Cu^-(H_2O)$.

$Cu^+(H_2O)$ channel, due to the variations of the signal in the initial 5–6 ps (Fig. 6), we only fit data at later times, using a sum of two exponentials for the fit,

$$I_{decay}(t) = I_2 e^{-t/\tau_2} + I_3 e^{-t/\tau_3}. \quad (9)$$

This functional form provides a good representation of the experimental data for $t > 2$ ps, but the fit is not at all sensitive to the exact value of t_0, which is determined only from the rise of the Cu^+ signal. Several data sets are analyzed for each of the two channels and the optimal values of the fit parameters are presented in Table I, where the uncertainties also include the variation of the fit parameters from data set to data set. We make two observations despite the large uncertainties resulting from the scatter in our data. First, the three characteristic time constants τ_1, τ_2, and τ_3 are each separated by an order of magnitude. Second, neither the time constants nor the weightings of each term in the fits differ significantly between $Cu(H_2O)$ and $Cu(D_2O)$.

V. DISCUSSION

A series of interesting questions are raised by our experimental results. The first and most important question is the following: how do we understand the complicated dynamics of $Cu(H_2O)$ following electron photodetachment from its anion? This raises more specific questions including the following: what is the time scale of H_2O reorientation, and what are the specific energy transfer processes responsible for the three dissociation time scales that are observed? A series of related questions directly address the interpretation of our experimental results: why do we observe the same time evolution of the $Cu^+(H_2O)$ signals when we probe at different wavelengths in the range 315–345 nm; how can we understand the immediate onset of the $Cu^+(H_2O)$ signals (the prompt ionization); how can we understand the variation of the $Cu^+(H_2O)$ signals in the first 5–6 ps; and why is two-color (327+265 nm) ionization of CuH_2O inefficient compared to the one-color (327 nm), multiphoton ionization? Prior to analyzing the dynamics and answering the above questions, we must characterize the response of the system to our photodetachment and photoionization schemes.

A. Electron photodetachment of $Cu^-(H_2O)$

Electron photodetachment from $Cu^-(H_2O)$ with one 398 nm (3.12 eV) photon can access both the ground electronic state of the $Cu(H_2O)$ neutral, which correlates to the ^2S state of Cu $(3d^{10}4s)+H_2O$, and the first excited states, which correlate to the ^2D states of Cu $(3d^9 4s^2)+H_2O$. Negative ion photoelectron spectroscopy[37,38] has determined vertical photodetachment energies of 1.58 eV for the $Cu(H_2O)$ ground state and 2.92 eV for the first excited state manifold. Thus the present photodetachment energy is very close to the threshold for formation of the first excited states of $Cu(H_2O)$. Photoelectron imaging spectra of $Cu^-(H_2O)$ obtained with 410 nm radiation show that the excited state contribution to the photodetachment cross section is $<2\%$ of the total.[53] Calculations[54] of electron photodetachment from Cu^- also show that the excited state contribution is small. In addition, the resonant ionization scheme employed selectively probes ground-state $Cu(H_2O)$. Based upon all of these facts, we conclude that the excited state $Cu(H_2O)$ contributions to the transient cation signals are negligible.

B. Resonant photoionization of $Cu(H_2O)$

The possible processes that contribute to the cation signal must be clarified in order to extract the correct dynamical information from our experimental data. While there is no ambiguity concerning the two-color resonant ionization of the Cu neutral fragment (Fig. 3, scheme 2), we need a careful analysis of the possible processes that contribute to the one-color resonant multiphoton photoionization of the bound $Cu(H_2O)$ complex [Fig. 3, schemes 3(a) and 3(b)]. Our experimental results show that the two-color (OPA+265 nm) ionization of $Cu(H_2O)$ makes only a minor contribution to the $Cu^+(H_2O)$ cation signals when compared to the one-color (OPA, $\lambda = 315–345$ nm) multiphoton ionization, even though the 265 nm pulse typically has five times the number of photons as the 327 nm OPA pulse.

A possible explanation is that the one-color ionization of the $Cu(H_2O)$ complex prevails because it is a two-photon, resonant process, accessing a Rydberg state. Figure 8 shows that both the excitation ($^2P \leftarrow {}^2S$) and ionization energies of the $Cu(H_2O)$ complex vary significantly as a function of the Cu-(H_2O) radial separation and the orientation of the H_2O molecule. The complex can be resonantly excited at selected configurations over a range of OPA wavelengths centered on the Cu atom transition ($^2P_{1/2} \leftarrow {}^2S_{1/2}$ 327 nm, 3.79 eV). A second OPA photon of the same energy can only ionize selected $Cu(H_2O)$ configurations whereas a second photon of

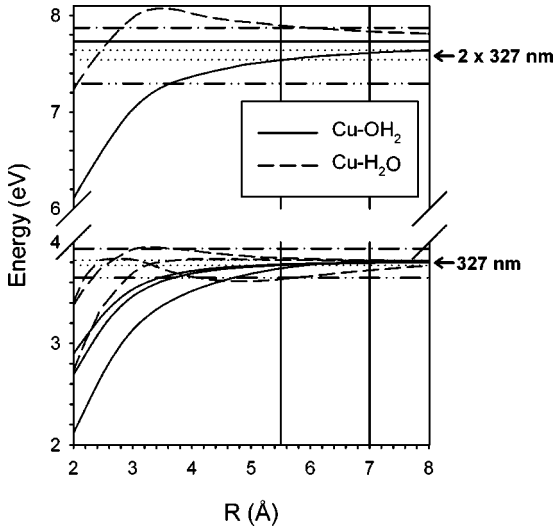

FIG. 8. $Cu(H_2O)$ vertical electronic excitation energy and ionization energy calculated as a function of the Cu-(H_2O) radial distance for the two C_{2v} orientations, Cu-OH_2 (solid lines) and Cu-H_2O (dashed lines). The horizontal lines show the FWHM energy spread of one and two 327 nm probe photons (dotted lines); the energies of one and two 315 nm (dash-dot lines) and 340 nm (dash-dot-dot lines) photons; and the ionization energy of Cu (7.726 eV) (solid line). The vertical lines illustrate the probe window used to calculate the cation signals for $Cu^+(H_2O)$ in Fig. 9.

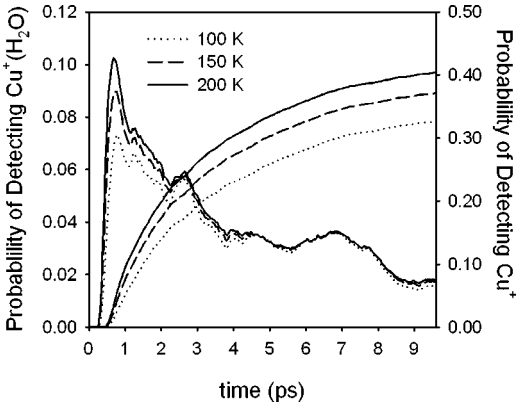

FIG. 9. Calculated probabilities of detecting Cu^+ and $Cu^+(H_2O)$ cation signals as a result of the quantum mechanical wave packet propagation calculations. The ionization detection windows assumed are 5.5–7 Å for the $Cu^+(H_2O)$ signal and >7 Å for the Cu^+ signal. Details of the calculations are presented in the text.

our third harmonic (265 nm, 4.68 eV) has enough energy to ionize all $Cu(H_2O)$ configurations. This suggests that there is increased probability of accessing Rydberg states of the neutral complex with two OPA photons in the range investigated (315–345 nm). These Rydberg states could then ionize through rotational autoionization,[55,56] utilizing the internal rotation of the H_2O dipole in the complex. This ionization process would involve a bound-bound transition, with a significantly larger cross section than the bound-free ionization when using the 265 nm as the second photon.

C. Comparison and analysis of the experimental and calculated Cu^+ and $Cu^+(H_2O)$ signals

In order to better address the remaining questions raised by our experimental results, we investigate the dynamics of $Cu(H_2O)$, following electron photodetachment of $Cu^-(H_2O)$, by quantum mechanical wave packet calculations. We use a simple model that is based on the curves in Fig. 8 to convert these time evolving wave packets into Cu^+ and $Cu^+(H_2O)$ signals. As the neutral potential surface is strongly attractive only at short Cu-H_2O distances, at Cu-H_2O separations that are larger than a threshold value, R_{Cu}, the complex is considered to be dissociated and the probability amplitude in this region will be taken to correspond to the probability of detecting Cu^+. In order to produce a $Cu^+(H_2O)$ signal, the energy difference between the ground and the excited states of the complex must match the energy of one 327 nm photon. Based on the plots in Fig. 8, this condition is satisfied for Cu-H_2O distances greater than 5.5 Å and the probability amplitude with $5.5\ \text{Å} < R < R_{Cu}$ will be equated with the probability for detecting $Cu^+(H_2O)$. The results are found to be relatively insensitive to the choice of R_{Cu}, and we have taken it to be 7 Å. In this analysis, we have assumed that the photoionization cross section is independent of the $Cu(H_2O)$ configuration. The above analysis is performed for each of the ten lowest energy states of $Cu^-(H_2O)$. These results are weighted by the appropriate Boltzmann factor to provide the signal for a given temperature.

In Fig. 9 we present the calculated probabilities of detecting Cu^+ and $Cu^+(H_2O)$ at three anion temperatures: 100, 150, and 200 K. There is an excellent agreement between the experimental and calculated Cu^+ and $Cu^+(H_2O)$ signals and the main features are accurately reproduced. The calculated signals have been fit to the model, given in Eqs. (8) and (9). The resulting time constants are reported in Table I and are in excellent agreement with the experimental values. As with the experimental constants, there is no difference in the time constants or amount of direct dissociation between $Cu(H_2O)$ and $Cu(D_2O)$ within uncertainties of the fit.

Having obtained good agreement between the experimental and calculated signals, we can analyze the sources of the various features in the experimental signal. The most notable features are the ones that occur at short times: the immediate onset of the $Cu^+(H_2O)$ signal, the initial peak in the $Cu^+(H_2O)$ signal, the rapid rise of the Cu^+ signal, and the delay between the onsets of the two signals.

When we place the anion wave functions onto the neutral surface, the average energy is above the dissociation limit for all but the ground state, where the average energy is $-14\ \text{cm}^{-1}$. As a result, a significant fraction of the wave packet rapidly spreads to large values of R. This corresponds to $Cu(H_2O)$ undergoing direct dissociation. This feature manifests itself in the initial peak in the $Cu^+(H_2O)$ in the calculated signals in Fig. 9. It is also reflected in the rapid rise of the Cu^+ signal, which is modeled by the tanh term in Eq. (8).

The fact that there is a strong temperature dependence on the peak at 0.5–1.0 ps in the $Cu^+(H_2O)$ signal reflects the initial population of the vibrational states of $Cu^-(H_2O)$. If we assume a Boltzmann distribution describes the relative populations of the vibrational states of $Cu^-(H_2O)$, at 100 K only 22% of the anions will have one or more quanta of

excitation in the Cu-H_2O stretch, while at 200 K, 44% of the states will have excitation in this mode.[35] Since the Cu-H_2O stretch in the anion correlates to dissociation on the neutral surface, a higher population of vibrationally excited states will lead to a larger fraction of the sample undergoing direct dissociation. This will lead to a larger initial rise in the $Cu^+(H_2O)$ signal at 0.5–1 ps and a faster rise of the Cu^+ signal. Likewise, the delay between the $Cu^+(H_2O)$ and Cu^+ onsets can be understood as the time required for the wave packet to reach a detection window at the large Cu-H_2O separations where the separated Cu atom can be resonantly photoionized.

A similar variation in the short-time behavior of the $Cu^+(H_2O)$ signals is seen in the experimental results, plotted in the inset in Fig. 6, and suggests that part of the day-to-day variation of the measured $Cu^+(H_2O)$ transients may be the result of variable conditions in the ion source, which are hard to control and result in anions with different temperatures on different days.

One short-time feature in the experimental signals that is not reproduced in the calculations is the immediate onset of detectable $Cu^+(H_2O)$. We believe that this signal arises from the rapid delocalization of the wave function along the two angular coordinates. As the calculated signal is based solely on the probability amplitude as a function of the Cu-H_2O distance, this source of $Cu^+(H_2O)$ signal is not reflected by the present model. On the other hand, the rapid onset can be understood from the results of the simulations. Figure 8 shows that the electronic excitation energy of Cu(H_2O) depends on the H_2O orientation. Specifically, at the $Cu^-(H_2O)$ equilibrium separation of 3.3 Å, two OPA photons in the wavelength range 315–345 nm have insufficient energy to ionize Cu(H_2O) in the Cu-H_2O geometries, but in configurations with the oxygen oriented toward the copper atom, Cu(H_2O) can be ionized. In Fig. 10, we plot the probability amplitude for various orientations of Cu(H_2O) as a function of time for an initial distribution of $Cu^-(H_2O)$ states which corresponds to a vibrational temperature of 150 K. The probabilities have been normalized by the corresponding values for an isotropic distribution. Initially, the wave packets are localized near $\phi=0°$ and $\theta=90°$, the most probable configuration of the anion.[35] After less than 75 fs, the probability amplitude is delocalized over all possible orientations. This is considerably less than the time resolution of our experiment, 0.26 ps, and thus we do not expect to resolve the reorientation of H_2O in the present experiments. Based on the above analysis, the results of the simulations are entirely consistent with the observed onset of the $Cu^+(H_2O)$ signal, although such an effect is not incorporated in the model used to obtain the plots in Fig. 9.

At longer times, the complex continues to dissociate, although at a slower rate. This is reflected in the I_2 contribution to the signals, which has an associated time constant of several picoseconds. As can be seen in Fig. 1, and more quantitatively in Fig. 4 of the following paper, the Cu(H_2O) surface is very anisotropic, especially at Cu-H_2O distances that are smaller than 3.0 Å. Further, analysis of the anion states show that, even in the ground state, the average kinetic energy in the two angular coordinates is 187 cm^{-1}. As the

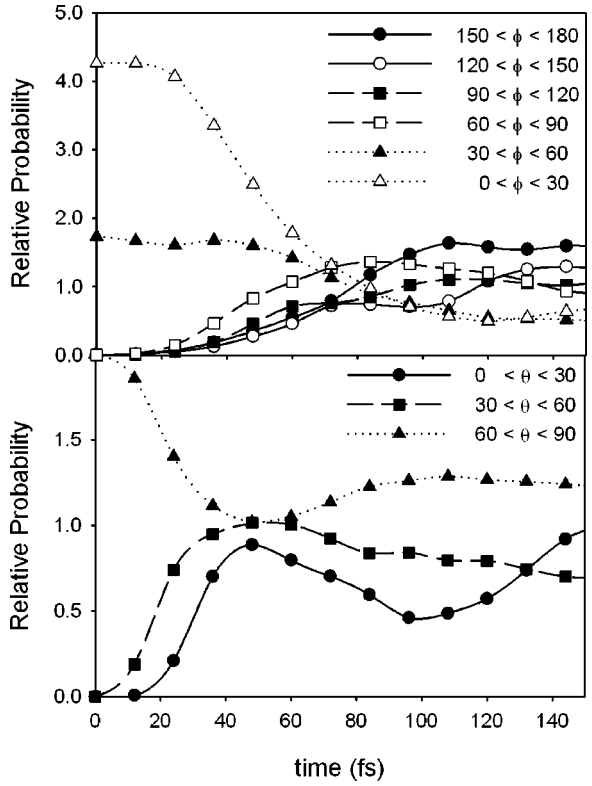

FIG. 10. Probability amplitudes integrated over (a) all values of R and θ and over the specified range of ϕ and (b) all values of R and ϕ and over the specified range of θ, plotted as a function of the propagation time and normalized to the values that would be obtained if the system were isotropic. The plotted distributions represent the sum of the values for specific initial states, weighted by the Boltzmann factors for a 150 K vibrational temperature of $Cu^-(H_2O)$.

wave packet is allowed to evolve in time, the kinetic and potential couplings between the radial and angular motions will lead to energy transfer between the rotations of the water molecule and the Cu-H_2O dissociation coordinate. It is this effect that is responsible for the intermediate time constants. Based on an analysis of the bound portion of the wave packet, the part with $R<7$ Å, we find that the average kinetic energy in the angular degrees of freedom is reduced by more than one-third after 10 ps. Since the total energy is conserved and the total energy is close to or above the dissociation threshold for the complex, the energy lost from the rotational motions must go into the Cu-H_2O dissociation coordinate.

A second question that is raised by this longer time behavior is the relative insensitivity of τ_2 to the wavelength of the OPA photon, at least over the range from 315 to 345 nm. Within our model, changing the energy of the probe photon will shift the regions of configuration space at which the energy of the OPA photon matches the differences between the energies of the ground and excited states of Cu(H_2O) and the energy difference between the excited state and $Cu^+(H_2O)$. While shifting the configurations at which $Cu^+(H_2O)$ and Cu^+ can be detected may lead to changes in the structure of the signals, the value of τ_2 reflects the rate that probability amplitude passes into and through regions of configurations space at which $Cu^+(H_2O)$ or Cu^+ can be

formed. As such, it is not expected to be affected by small changes in the locations of the probe windows brought about by changing the wavelength of the probe laser.

Finally, we note that tens of picoseconds after photodetachment, the complex continues to dissociate at a slower rate, with time constant of the order of 100 ps. This time scale is not accounted for by the 10 ps propagations. A likely source of this long-time decay is through vibrational predissociation out of vibrationally excited states of H_2O. From electronic structure calculations, we find that the H_2O geometry and vibrational frequencies differ slightly between the anion complex and in free H_2O.[35] Franck-Condon calculations based on the harmonic frequencies and geometries of the anion and neutral complexes suggest that, following electron photodetachment from $Cu^-(H_2O)$, about 10% of $Cu(H_2O)$ possess excitation of intramolecular H_2O vibrations.

VI. CONCLUSIONS

A detailed investigation of the time-dependent and dissociation dynamics of the $Cu(H_2O)$ complex has been performed through a combination of experiment and theory. The experimental dynamics is initiated through electron photodetachment from the anion, a defined starting point that provides an initial neutral complex with significant vibrational excitation in the Cu-H_2O intermolecular modes. The dynamics is probed through time-delayed resonant multiphoton ionization, a sensitive probe of structural dynamics in the complex. In parallel, the dynamics of the system is also investigated theoretically, through quantum mechanical wave packet calculations.

The excellent agreement between the results of the wave packet calculations and the experimental data enables us to extract detailed physical information about the $Cu(H_2O)$ dynamics from the calculations. The conclusions that are supported by the experimental results indicate that following electron photodetachment from $Cu^-(H_2O)$, the H_2O rotates and angularly delocalizes faster than our experimental time resolution (260 fs). The nascent $Cu(H_2O)$ neutral undergoes rearrangement and dissociation. Dissociation occurs on several distinct time scales. We identify a direct component (0.6 ps) that originates from anions with excitation in the intermolecular Cu-H_2O stretch. A second time scale (8 ps) of delayed dissociation arises from energy transfer from H_2O internal rotation to the Cu-H_2O dissociation coordinate. A third dissociation time scale (100 ps) is proposed to arise from the vibrational predissociation of complexes possessing excitation of the intramolecular vibrations of H_2O.

The information gained from this detailed analysis of the dynamics of $Cu(H_2O)$ will add to the interpretation of more complex systems that we envision studying in the future. Larger $Cu(H_2O)_n$ clusters are an immediate extrapolation and the investigation of their femtosecond dynamics is currently in progress. Compelling future candidates include metal-ligand systems with heavier ligands, in which the slower ligand motion may be resolvable by our experiments. Finally, we are experimenting with entrainment and argon cooling techniques[57,58] for generating colder anions, which will simplify the interpretation of the neutral dynamics.

ACKNOWLEDGMENTS

We gratefully acknowledge support from the National Science Foundation under Grant Nos. CHE0201848 and PHY0096822 (W.C.L.) and CHE-0200968 (A.B.M.), and the Air Force Office of Scientific Research Grant No. F49620-02-1-0371 (W.C.L.). A.B.M. was supported by the JILA Visiting Fellowship program. F.M. thanks Chris H. Greene for enlightening discussions on the experimental results. A.B.M. also acknowledges the Dreyfus Foundation awards program for partial support of this work.

[1] J. C. Owrutsky, D. Raftery, and R. M. Hochstrasser, Annu. Rev. Phys. Chem. **45**, 519 (1994).
[2] G. A. Voth and R. M. Hochstrasser, J. Phys. Chem. **100**, 13034 (1996).
[3] J. T. Hynes, in *Ultrafast Dynamics of Chemical Systems*, edited by J. D. Simons (Dordrecht, Boston, 1994), Vol. 7, p. 345.
[4] J. T. Hynes, in *Solvent Effects and Chemical Reactivity*, edited by O. Tapia and J. Bertrán (Kluwer Academic, Boston, 1996), Vol. 17, p. 231.
[5] M. Maroncelli, J. Mol. Liq. **57**, 1 (1993).
[6] R. Jimenez, G. R. Fleming, P. V. Kumar, and M. Maroncelli, Nature (London) **369**, 471 (1994).
[7] R. M. Stratt and M. Maroncelli, J. Phys. Chem. **100**, 12981 (1996).
[8] J. A. Syage and A. H. Zewail, Adv. Mol. Vib. Collision Dyn. **3**, 1 (1998).
[9] Q. Zhong and A. W. Castleman, Jr., Chem. Rev. (Washington, D.C.) **100**, 4039 (2000).
[10] R. Parson, N. Delaney, A. Sanov, and W. C. Lineberger, in *Physics and Chemistry of Clusters, Proceedings of Nobel Symposium 117*, edited by E. E. B. Campbell and M. Larsson (World Scientific, Singapore, 2001), p. 132.
[11] D. M. Neumark, Annu. Rev. Phys. Chem. **52**, 255 (2001).
[12] A. Sanov and W. C. Lineberger, PhysChemComm **5**, 165 (2002).
[13] D. H. Paik, T. M. Bernhardt, N. J. Kim, and A. H. Zewail, J. Chem. Phys. **115**, 612 (2001).
[14] D. H. Paik, N. J. Kim, and A. H. Zewail, J. Chem. Phys. **118**, 6923 (2003).
[15] N. J. Kim, D. H. Paik, and A. H. Zewail, J. Chem. Phys. **118**, 6930 (2003).
[16] M. Roeselova, U. Kaidor, and P. Jungwirth, J. Phys. Chem. A **104**, 6523 (2000).
[17] M. Roeselova, M. Mucha, B. Schmidt, and P. Jungwirth, J. Phys. Chem. A **106**, 12229 (2002).
[18] L. Krim, P. Qiu, N. Halberstadt, B. Soep, and J. P. Visticot, in *Femtosecond Chemistry* (VCH, Weinheim, Germany, 1995), Vol. 2, p. 433.
[19] C. R. Sherwood, M. C. Garner, K. A. Hanold, K. M. Strong, and R. E. Continetti, J. Chem. Phys. **102**, 6949 (1995).
[20] K. A. Hanold, M. C. Garner, and R. E. Continetti, Phys. Rev. Lett. **77**, 3335 (1996).
[21] K. A. Hanold, A. K. Luong, T. G. Clements, and R. E. Continetti, Rev. Sci. Instrum. **70**, 2268 (1999).
[22] R. E. Continetti, Annu. Rev. Phys. Chem. **52**, 165 (2001).
[23] C. R. Sherwood and R. E. Continetti, Chem. Phys. Lett. **258**, 171 (1996).
[24] A. K. Luong, T. G. Clements, and R. E. Continetti, J. Phys. Chem. A **103**, 10237 (1999).
[25] H. J. Deyerl, A. K. Luong, T. G. Clements, and R. E. Continetti, Faraday Discuss. **115**, 147 (2000).
[26] A. K. Luong, T. G. Clements, M. S. Resat, and R. E. Continetti, J. Chem. Phys. **114**, 3449 (2001).
[27] T. G. Clements, A. K. Luong, H. J. Deyerl, and R. E. Continetti, J. Chem. Phys. **114**, 8436 (2001).
[28] A. Materny, T. Chen, M. Schmitt, T. Siebert, A. Vierheilig, V. Engel, and W. Kiefer, Appl. Phys. B: Lasers Opt. **71**, 299 (2000).
[29] M. Dantus, Annu. Rev. Phys. Chem. **52**, 639 (2001).
[30] S. Wolf, G. Sommerer, S. Rutz, E. Schreiber, T. Leisner, L. Wöste, and R. S. Berry, Phys. Rev. Lett. **74**, 4177 (1995).
[31] D. W. Boo, Y. Ozaki, L. H. Andersen, and W. C. Lineberger, J. Phys. Chem. A **101**, 6688 (1997).
[32] M. Hartmann, J. Pittner, V. Bonačić-Koutecký, A. Heidenreich, and J. Jortner, J. Chem. Phys. **108**, 3096 (1998).
[33] M. Hartmann, A. Heidenreich, J. Pittner, V. Bonačić-Koutecký, and J. Jortner, J. Phys. Chem. A **102**, 4069 (1998).
[34] E. A. A. Jarvis, E. Fattal, A. J. R. Da Silva, and E. A. Carter, J. Phys. Chem. A **104**, 2333 (2000).

[35] M. S. Taylor, A. B. McCoy, F. Muntean, and W. C. Lineberger, J. Chem. Phys. **121**, 5688 (2004), following paper.
[36] C.-G. Zhan and S. Iwata, Chem. Phys. Lett. **232**, 72 (1995).
[37] F. Misaizu, K. Tsukamato, M. Sanekata, and K. Fuke, Laser Chem. **15**, 195 (1995).
[38] F. Misaizu, K. Tsukamoto, M. Sanekata, and K. Fuke, Surf. Rev. Lett. **3**, 405 (1996).
[39] C. Nitsch, C. Hüglin, I. V. Hertel, and C. P. Schulz, J. Chem. Phys. **101**, 6559 (1994).
[40] C. P. Schulz and C. Nitsch, J. Chem. Phys. **107**, 9794 (1997).
[41] P. Brockhaus, I. V. Hertel, and C. P. Schulz, J. Chem. Phys. **110**, 393 (1999).
[42] R. Takasu, K. Nishikawa, N. Miura, A. Sabu, K. Hashimoto, C. P. Schulz, I. V. Hertel, and K. Fuke, J. Phys. Chem. A **105**, 6602 (2001).
[43] P. J. Campagnola, L. A. Posey, and M. A. Johnson, J. Chem. Phys. **95**, 7998 (1991).
[44] V. Vorsa, P. J. Campagnola, S. Nandi, M. Larsson, and W. C. Lineberger, J. Chem. Phys. **105**, 2298 (1996).
[45] W. C. Wiley and I. H. McLaren, J. Mass Spectrom. **32**, 4 (1997).
[46] The potential energy curves shown in Fig. 3 are based upon the full calculations described in the following paper.
[47] D. Kosloff and R. Kosloff, J. Comput. Phys. **52**, 35 (1983).
[48] R. Kosloff, J. Phys. Chem. **92**, 2087 (1988).
[49] R. Kosloff, in *Dynamics of Molecules and Chemical Reactions*, edited by R. E. Wyatt and J. Z. H. Zhang (Marcel Dekker, New York, 1996), p. 185.
[50] C. Leforestier, R. H. Bisseling, C. Cerjan *et al.*, J. Comput. Phys. **94**, 59 (1991).
[51] H. Tal-Ezer, R. Kosloff, and C. Cerjan, J. Comput. Phys. **100**, 179 (1992).
[52] S. K. Gray and G. G. Balint-Kurti, J. Chem. Phys. **108**, 950 (1998).
[53] T. Sanford, D. Andrews, J. Rathbone, and W. C. Lineberger (unpublished).
[54] K. F. Scheibner and A. U. Hazi, Phys. Rev. A **38**, 539 (1988).
[55] T. P. Softley, S. R. MacKenzie, F. Merkt, D. Rolland, D. M. Neumark, R. D. Levine, B. Kohler, and M. S. Child, XXth Solvay Conference on Chemistry, 1997, Vol. 101, pp. 667.
[56] F. Merkt, Annu. Rev. Phys. Chem. **48**, 675 (1997).
[57] W. H. Robertson, J. A. Kelley, and M. A. Johnson, Rev. Sci. Instrum. **71**, 4431 (2000).
[58] W. H. Robertson and M. A. Johnson, Annu. Rev. Phys. Chem. **54**, 173 (2003).